Available online at www.sciencedirect.com
ScienceDirect
Journal of Power Sources 167 (2007) 185–191
JOURNAL OF POWER SOURCES
www.elsevier.com/locate/jpowsour

Preparation and characterization of sub-micro $LiNi_{0.5-x}Mn_{1.5+x}O_4$ for 5 V cathode materials synthesized by an ultrasonic-assisted co-precipitation method

Ting-Feng Yi *, Xin-Guo Hu

Department of Applied Chemistry, Harbin Institute of Technology, Harbin 150001, PR China

Received 29 September 2006; received in revised form 3 February 2007; accepted 6 February 2007
Available online 13 February 2007

Abstract

Sub-micro spinel $LiNi_{0.5-x}Mn_{1.5+x}O_4$ ($x<0.1$) cathode materials powder was successfully synthesized by the ultrasonic-assisted co-precipitation (UACP) method. The structure and electrochemical performance of this as-prepared powder were characterized by powder XRD, SEM, XPS, CV and the galvanostatic charge–discharge test in detail. XRD shows that there is a small $Li_yNi_{1-y}O$ impurity peak placed close to the (4 0 0) line of the spinel $LiNi_{0.5-x}Mn_{1.5+x}O_4$, and the powders are well crystallized. XPS exhibits that the Mn oxidation state is between +3 and +4, and Ni oxidation state is +2 in $LiNi_{0.5-x}Mn_{1.5+x}O_4$. SEM shows that the prepared powders (UACP) have the uniform and narrow size distribution which is less than 200 nm. Galvanostatic charge–discharge test indicates that the initial discharge capacities for the $LiNi_{0.5-x}Mn_{1.5+x}O_4$ (UACP) at *C*/3, 1*C* and 2*C*, are 130.2, 119.0 and 110.0 mAh g^{-1}, respectively. After 100 cycles, their capacity retentions are 99.8%, 88.2%, and 73.5%, respectively. $LiNi_{0.5-x}Mn_{1.5+x}O_4$ (UACP) at *C*/3 discharge rate exhibits superior capacity retention upon cycling, and it also shows well high current discharge performance. CV curve implies that $LiNi_{0.5-x}Mn_{1.5+x}O_4$ ($x<0.1$) spinel synthesized by ultrasonic-assisted co-precipitation method has both reversibility and cycle capability because of the ultrasonic-catalysis.

Keywords: Lithium-ion battery; $LiNi_{0.5-x}Mn_{1.5+x}O_4$; Preparation; Charge–discharge performance; Ultrasonic-assisted co-precipitation method

1. Introduction

Several research groups have reported that transition metal-substituted spinel materials ($LiM_xMn_{2-x}O_4$, M = Ni, Cr, Co, Fe, Cu) are superior to $LiMn_2O_4$ due to the high-voltage plateaus above 4.5 V [1–5]. Among these materials, $LiNi_{0.5-x}Mn_{1.5+x}O_4$ ($x<0.1$) is the most promising and attractive one because of its acceptable stability, dominant potential plateau at around 4.7 V, good cyclic property and relatively high capacity with a plateau at around 4.7 V [6,7]. A variety of methods had been used to prepare $LiNi_{0.5-x}Mn_{1.5+x}O_4$ yet, such as solid-state reaction [6], sol–gel [8], emulsion drying [9], composite carbonate process [10], molten salt [11], combustion and ultrasonic spray pyrolysis method [12]. However, some problems impede such methods mentioned above from practical application. Solid-state method needs preheating, regrinding and extended high temperature calcinations to form a highly ordered phase that shows higher capacity. Although the other methods, such as sol–gel, emulsion drying and molten salt, etc., can overcome the disadvantages of solid-state method, they also have some other disadvantages, such as complicated synthetic routes and high synthetic cost, which is difficult for commercial applications. Therefore, it is very significant for a low-cost method to synthesize the homogenous precursors and the final product of $LiNi_{0.5-x}Mn_{1.5+x}O_4$ ($x<0.1$). In addition, ultrasonic has been applied to synthesize spinel lithium manganese oxide. Shen et al. [13] have reported that good stoichiometric control of $LiCr_xMn_{2-x}O_4$ spinel with uniform particle size distribution can be obtained by an ultrasonic bath; our groups [14] also have reported that spinel $LiAl_{0.05}Mn_{1.95}O_4$ powder with the uniform, nearly cubic structure and octahedral morphology with narrow size distribution can be obtained by ultrasonic-assisted sol–gel method. Hence, ultrasonic-assisted method is an effective method to prepare cathode material for lithium-ion

* Corresponding author. Tel.: +86 451 8641 3751; fax: +86 451 8622 1048.
E-mail address: tfyihit@hit.edu.cn (T.-F. Yi).

0378-7753/$ – see front matter © 2007 Elsevier B.V. All rights reserved.
doi:10.1016/j.jpowsour.2007.02.003

batteries with a simple process which has better structure and electrochemical performance. With this consideration, we introduce a low-cost method, ultrasonic-assisted co-precipitation method, to obtain sub-micro spinel $LiNi_{0.5-x}Mn_{1.5+x}O_4$ ($x<0.1$) cathode materials with homogeneous particle size, and the structure, morphology and electrochemical properties of spinel $LiNi_{0.5-x}Mn_{1.5+x}O_4$ ($x<0.1$) were studied through XRD, SEM, XPS, CV, and galvanostatic charge–discharge test, respectively.

2. Experimental

2.1. Materials preparation

$LiNi_{0.5-x}Mn_{1.5+x}O_4$ ($x<0.1$) powders were synthesized by reacting a stoichiometric mixture of $LiNO_3$ (AR, 99%), $Mn(NO_3)_2$ (AR, 50% solution), and $Ni(NO_3)_2{\cdot}6H_2O$(AR, 99%). The above chemicals were mixed at a predetermined molar ratio of Li:Mn:Ni = 1:1.5:0.5, and then in distilled water. The pH of the mixed solution was maintained 7.5 by adding ammonium hydroxide solution. After shocked at 80 °C for 5 h in a homemade mini ultrasonic claner (50 W, 28 kHz), the excess water was removed and the metal precipitate was formed. The metal precipitate so formed was dried in vacuum drying oven for 12 h at 110 °C. Then the precursors were heat treated at 800 °C for 24 h at ambient condition, and then air-cooled to the room temperature, yielding dark powders.

2.2. Materials characterization

Powder X-ray diffraction (XRD) was performed on Rigaku D/MAX-RC X-ray diffractometer with Cu $K\alpha_1$ (45 kV, 50 mA, step size = 0.02°, $10° < 2\theta < 80°$) monochromated radiation in order to identify the crystalline phase of the materials. The particle morphologies of the samples were examined with a scanning electron microscope (SEM, Hitachi, S-570). X-ray photoelectron spectroscopy (XPS) was performed on American PHI5700 ESCA with a non-monochromatic Mg Kα (1253.6 eV) light source to study the Mn and Ni oxidation states of materials. The C 1s XPS at 284.62 eV was used as the calibration of the spectra. Cyclic voltammetry (CV) was measured on an electrochemical workstation (CHI 630A) at a scan rate of 0.1 mV s^{-1} between 3.5 and 5 V (versus Li/Li^+). Charge–discharge performance of the cell was characterized galvanostatically on BTS 5 V/5 mA battery testing system (Shenzhen, China) at *C*/3 charge rate and *C*/3, 1*C*, and 2*C* discharge rates between 3.5 and 4.95 V (versus Li/Li^+), respectively.

2.3. Preparation of lithium-ion batteries

Slurry was formed by mixing the active material (85%), acetylene black (10%) and binder (5 wt.% polyvinylidene fluoride, PVDF, dissolved in *N*-methyl-2-pyrrolidone, NMP). The mixed slurry was coated onto an aluminum current collector. The electrodes were dried under vacuum at 120 °C overnight and then punched and weighed. The batteries were assembled in a glove box under a dry and high purity argon atmosphere (99.999%). The complete coin cell comprises a cathode, a celgard 2300 (polypropylene) as the separator and lithium foil anode. One molar of $LiPF_6$ (battery grade) dissolved in a mixture of ethylene carbonate (EC, battery grade) and dimethyl carbonate (DMC, battery grade) (1:1 by volume) was used as the electrolyte.

3. Results and discussion

3.1. XRD analysis

The XRD patterns of the $LiNi_{0.5-x}Mn_{1.5+x}O_4$ ($x<0.1$) samples (UACP) are presented in Fig. 1.

The main peaks for these prepared materials are labeled with *h k l* indexes. All of the diffraction peaks are assigned to the spinel compound $LiNi_{0.5-x}Mn_{1.5+x}O_4$ ($x<0.1$), and the results are in good accordance with the standard spectra (JCPDS, Card No. 35-0782). It has been reported [7] that $LiNi_{0.5}Mn_{1.5}O_4$ losses oxygen and disproportionates to a spinel and $Li_yNi_{1-y}O$ when it is heated above 650 °C. So it is difficult to obtain stoichiometric $LiNi_{0.5}Mn_{1.5}O_4$ spinels. Small $Li_yNi_{1-y}O$ impurity peak placed close to the (4 0 0) line of the spinel denoted by asterisk is also observed in Fig. 1. The formation of the $Li_yNi_{1-y}O$ impurity phase can be shown by the generalized reaction:

$$LiMn_{1.5}Ni_{0.5}O_4 \rightarrow \alpha Li_yNi_{1-y}O + \beta LiMn_{1.5+x}Ni_{0.5-x}O_4 + \gamma O_2$$

where α, β and γ define, respectively, the relative amounts of the $Li_yNi_{1-y}O$, $LiNi_{0.5-x}Mn_{1.5+x}O_4$, and O_2 phase.

Anyway, the integration of the XRD pattern shows that the content of $Li_yNi_{1-y}O$ is ca. 1% of the total spinel phase from the diffractograms according to the peak area comparison, and thus its effect in the electrochemical curves can be neglected [15]. All fundamental peaks are sharp, which indicates that the prepared powders are well crystallized. The intensity ratio of the two peaks, $I(3\,1\,1)/I(4\,0\,0)$, is closely related to the electrochemical properties of spinel lithium manganese oxide [16,17]. For example, Al doped Li–Mn–O spinel compounds with the $I(3\,1\,1)/I(4\,0\,0)$ ratios between 0.96 and 1.1 have shown better electrochemical properties than those outside this region [17]. In this study, the $I(3\,1\,1)/I(4\,0\,0)$ ratio value of the samples is 0.98,

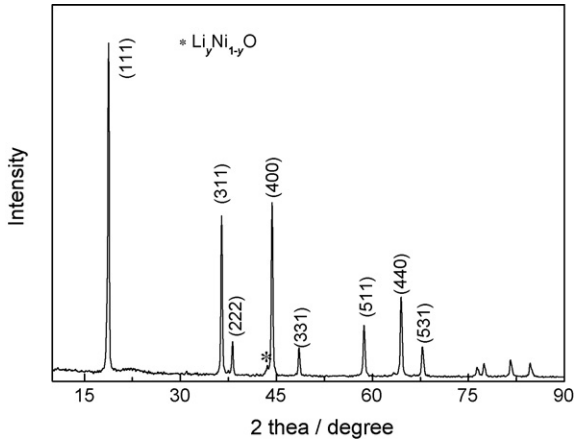

Fig. 1. X-ray powder diffraction patterns obtained from the prepared samples of $LiNi_{0.5-x}Mn_{1.5+x}O_4$.

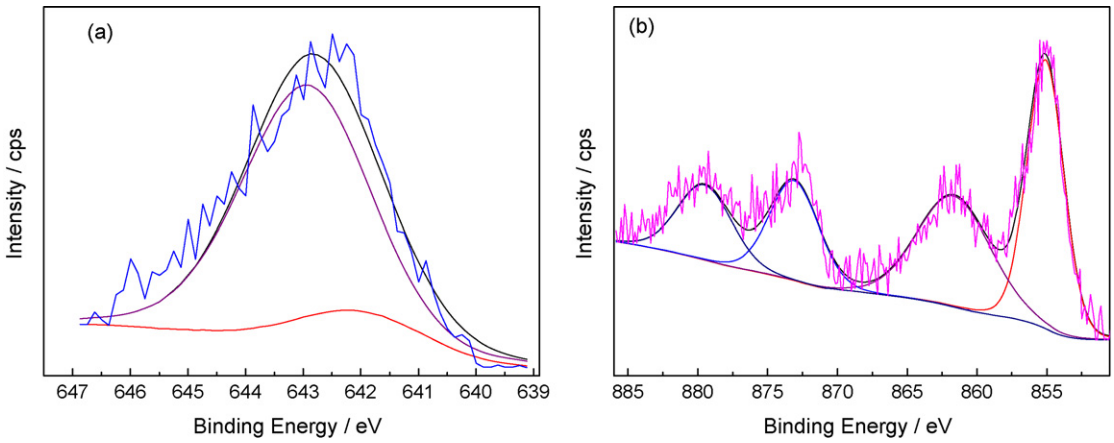

Fig. 2. XPS spectra of (a) Mn 2p and (b) Ni 2p for the prepared samples of $LiNi_{0.5-x}Mn_{1.5+x}O_4$ spinel.

which is comparable with that of Al doped Li–Mn–O spinel compounds. Furthermore, the oxides $Li_yNi_{1-y}O$ ($0 < y \leq 0.3$) have little activities as cathode materials for lithium-ion batteries [18]. Therefore, it is reasonable that the $LiNi_{0.5-x}Mn_{1.5+x}O_4$ material is expected to show better electrochemical performance. For the $LiNi_{0.5-x}Mn_{1.5+x}O_4$ spinel, the lattice constant calculated through the least square program method using the internal Si reference is 8.1682 Å. The increase in amount of Mn^{4+}–O bond which is shorter than that of Mn^{3+}–O bond, leads to the shrinkage of the spinel framework, resulting in smaller lattice constants than that of $LiMn_2O_4$. The volume change during the cycling process may be suppressed by this way. The aforementioned features of Li–Mn–Ni–O spinel are very desirable for being employed as the electrode material to improve the electrochemical properties for lithium rechargeable batteries.

3.2. XPS analysis

The Mn 2p and Ni 2p XPS spectra of $LiNi_{0.5-x}Mn_{1.5+x}O_4$ spinel are given in Fig. 2, and the XPS spectra for the spinel $LiNi_{0.5-x}Mn_{1.5+x}O_4$ are plotted in Fig. 3. The BE (binding energy) values are accurate within ±0.1 eV. The spectra of the Mn 2p can be deconvoluted into two peaks, the dominant one with a BE of 642.9 eV (corresponds to Mn^{4+}) and the other with 641.9 eV (corresponds to Mn^{3+}). These values may be compared with 641.7 eV for Mn^{3+} in $LiMn_2O_4$ [19] and 641.8 eV for Mn^{3+} in Mn_2O_3 [20]. Our value for Mn^{4+} is close to the reported value of 642.7 eV for $LiMn_2O_4$ [19] and 642.6 and 642.5 eV for MnO_2 [20–22]. However, the value for Mn^{4+} is lower than the reported value of 643.2 eV for $LiCo_{0.15}Mn_{0.85}O_2$ [23]. This indicates the Mn oxidation state in $LiNi_{0.5-x}Mn_{1.5+x}O_4$ is between +3 and +4, and the relative amounts of Mn^{3+} and Mn^{4+} estimated from the area under the peaks are 10% and 90% (0.15 Mn^{3+} and 1.35 Mn^{4+}), respectively. Therefore, the Jahn–Teller distortion is restrained which is ascribed to the low Mn^{3+}/Mn^{4+} ratio. The peak at 49.8 eV in the above compound can be assigned to Mn 3p [24]. The Ni 2p spectra for the spinel materials are shown in Fig. 2(b). Ni $2p_{3/2}$ has an only one BE at 855.0 eV which can be ascribed to Ni^{2+} ions at octahedral sites in the spinel structure. This value is consistent with those reported for $LiNi_{0.5}Mn_{1.5}O_4$ (855.1 eV) [25] and other Ni and Mn spinels (e.g., 855.2 eV for $NiMn_2O_4$) [26]. The result reveals that the Ni oxidation state in $Li_yNi_{1-y}O$ and $LiNi_{0.5-x}Mn_{1.5+x}O_4$ is +2. The Li 1s spectra for the spinel materials which shows peak at 53.8 eV are unclear in Fig. 3, indicating that the Li 1s spectra are covered by Mn 3p and Ni 3p due to the small X-ray scattering factor of lithium. The value is comparable to those for Li in $LiMn_2O_4$ (about 55 eV) [21] and in $LiNiO_2$ (53.7 eV) [27]. The peaks at 530.6 eV noted, for the spinel $LiNi_{0.5-x}Mn_{1.5+x}O_4$ is in agreement with the BE value of 529–530 eV for O 1s in $LiMn_2O_4$ and $LiNiO_2$ [21,27]. The origin of peaks at 530.6 eV observed at higher binding energies can be ascribed to either OH^- groups, O^{2-}, or the multiplicity of physisorbed and chemisorbed water on and into the surface.

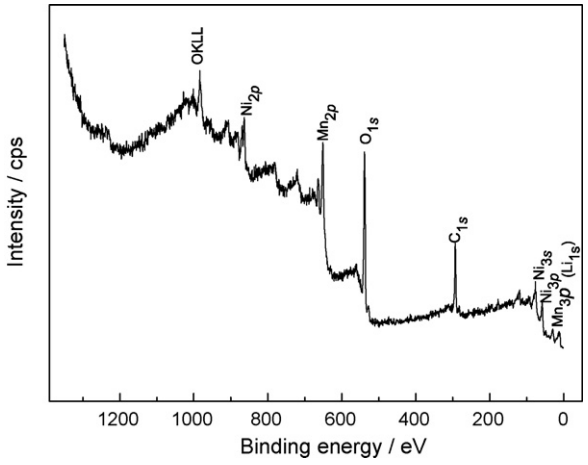

Fig. 3. XPS spectra for the spinel $LiNi_{0.5-x}Mn_{1.5+x}O_4$.

3.3. SEM analysis

Typical SEM photographs of $LiNi_{0.5-x}Mn_{1.5+x}O_4$ ($x < 0.1$) prepared by different methods are shown in Fig. 4.

However, there is greater extent of agglomeration of particles in the $LiNi_{0.5-x}Mn_{1.5+x}O_4$ samples synthesized by co-precipitation method, and the $LiNi_{0.5-x}Mn_{1.5+x}O_4$ samples obtained from co-precipitation method have bigger particle size

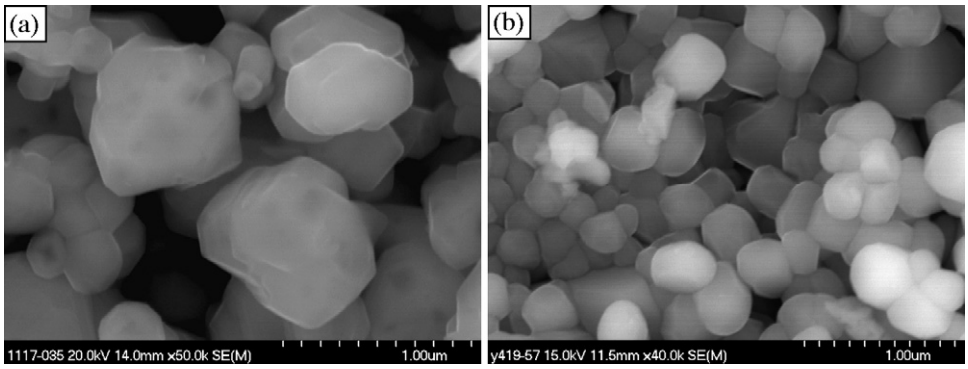

Fig. 4. Typical scanning electron micrographs (SEM) of $LiNi_{0.5-x}Mn_{1.5+x}O_4$ ($x<0.1$) cathode material prepared by (a) co-precipitation method; (b) ultrasonic-assisted co-precipitation method.

(about 500 nm) than that of $LiNi_{0.5-x}Mn_{1.5+x}O_4$ samples (about 200 nm) obtained from UACP method. The results indicate that the ultrasonic process can make the solid powders dispersed more uniformly in the liquid substances and to some extent effectively restrain the agglomeration of solid powders. The results indicate that the ultrasonic-assisted co-precipitation is a useful method for the synthesis of homogenous precursors, narrow and uniform particle size distributions in the final products. The aforementioned features of $LiNi_{0.5-x}Mn_{1.5+x}O_4$ cathode materials (UACP) are very desirable for being employed as the electrode material to improve the electrochemical properties of lithium rechargeable batteries.

3.4. Electrochemical performance

The initial charge–discharge curves in a potential range from 3.5 to 4.95 V of $LiNi_{0.5-x}Mn_{1.5+x}O_4$ ($x<0.1$) (UACP) are shown in Fig. 5. The upper limit was set at 4.95 V to avoid increasing the charge capacity by effect of side reactions such as the release of oxygen from the spinel lattice above 5.0 V [28].

All curves were obtained at *C*/3 charge rate, and the discharge curves were obtained at *C*/3, 1*C*, and 2*C* rates, respectively. All discharge and charge curves have two potential plateaus at 4.0 and 4.7 V. With increasing the discharge rate, the discharge capacity descend quickly, and the discharge potential and discharge plateaus also change a lot, which the 4.7 V discharge voltage plateaus decrease and 4 V plateaus nearly disappears. The amount of Ni deficiency can be presumably estimated from the length of 4.1 V plateau (*C*/3 discharge rate). We estimate that a Ni concentration of $0.5-x$ is about 0.45 in this sample. Charge–discharge reactions into/from spinel $LiNi_{0.5}Mn_{1.5}O_4$ proceeds reversibly according to the following equation:

$$Li[Ni_{1/2}Mn_{3/2}]O_4 \underset{\text{Discharge}}{\overset{\text{Charge}}{\rightleftharpoons}} Li_{1-x}[Ni_{1/2}Mn_{3/2}]O_4 + xLi + xe$$

So far, it has been proposed that a substitution of Mn ions in $LiMn_2O_4$ originates a 5 V potential plateau and a kind of substitution ion influences on 5 V behavior of $LiNi_xMn_{2-x}O_4$ cathode materials. Several researchers have claimed that an energy level of d-electron in Ni ion is responsible for 5 V discharge potential [7,29]. One of explanations for 5 V potential may be suggested as follows. Fig. 6 shows a proposed diagram of electronic levels in the system of Mn^{3+} and Ni^{2+} ions. In terms of the proposed diagram of electronic structure in $LiNi_xMn_{2-x}O_4$ during the charging process, electrons are taken from the manganese e_g level, and, after being used up, are taken from the e_g level of nickel. A binding energy of electron in e_g level of Mn and Ni ions are estimated to be 1.5–1.6 eV and 2.1 eV, respectively, with respect to that in t_{2g} level of Mn^{3+} ion [29]. This is accompanied by a step lowering of the Fermi level by the 0.5–0.6 eV, reflected as the 0.5–0.6 V jump in the $Li/LiNi_xMn_{2-x}O_4$ cathode potential. This leads to a higher discharge and charge potential. From energy levels of d-orbital in Mn and Ni ions, it can be expected that 4 V potential plateau corresponds to the redox couple of Mn^{3+}/Mn^{4+} and 5 V potential ones are due to two redox cou-

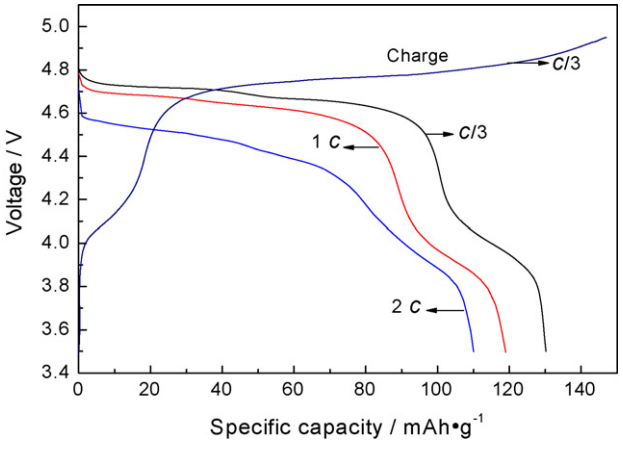

Fig. 5. Voltage (V)-specific capacity ($mAh\,g^{-1}$) profiles obtained from $LiNi_{0.5-x}Mn_{1.5+x}O_4$ ($x<0.1$) during charge–discharge step in the 3.5–4.95 V region in the first cycle.

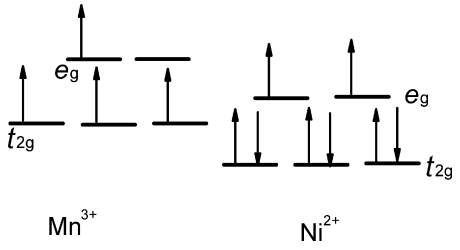

Fig. 6. Diagram of electronic levels for nickel-doped manganese spinel from Ref. [4].

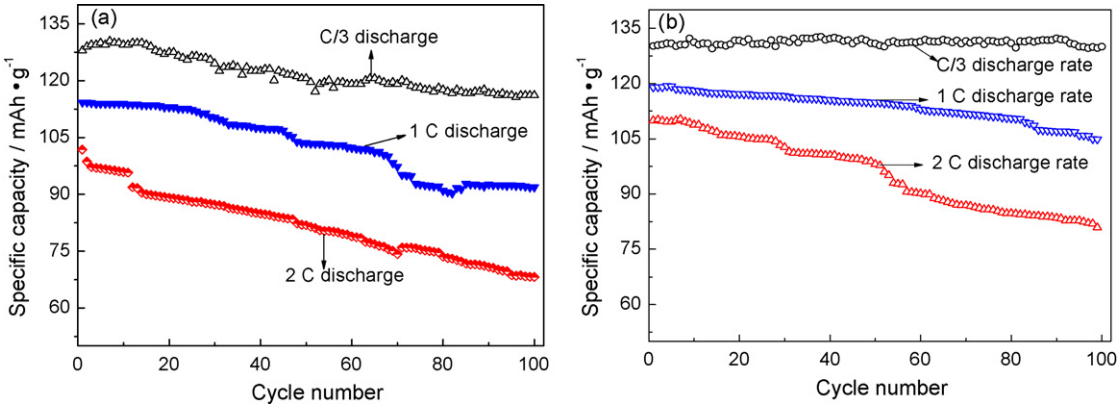

Fig. 7. Capacity vs. cycle number for $LiNi_{0.5-x}Mn_{1.5+x}O_4$ ($x<0.1$) synthesized by (a) co-precipitation method; (b) ultrasonic-assisted co-precipitation method at different discharge rates between 3.5 and 4.95 V.

ples of Ni^{2+}/Ni^{3+} and Ni^{3+}/Ni^{4+}. The discharge curve at 5 V involved two plateaus. The lower potential plateau is assigned to the Ni^{2+}/Ni^{3+} redox couple and the higher one is contributed by the Ni^{3+}/Ni^{4+} redox.

In order to study the influence of doping Ni^{2+} ions and synthesis method on the cycleability of spinel $LiNi_xMn_{2-x}O_4$ ($x<0.1$), the result of the cycle profiles of Ni-doped spinel is illustrated in Fig. 7. Table 1 summarizes the cycling performance of the prepared powders discharged at different current densities from Fig. 7. Compared with the $LiNi_xMn_{2-x}O_4$ synthesized by co-precipitation method, the Ni-doped spinel obtained from the simple UACP method has a larger initial discharge capacity and much higher capacity retention rate at different discharge rates after 100 cycles as shown in Table 1, which is due to be related with its better crystallinity and regular morphology, also this comment is well consistent with the SEM results mentioned above. $LiNi_xMn_{2-x}O_4$ (UACP) at *C*/3 discharge rate exhibits superior capacity retention upon cycling, and it also shows well high current discharge performance. Combining this with the electrochemical behavior, it can be concluded that the structure of $LiNi_xMn_{2-x}O_4$ synthesized by the UACP method is very stable for lithium ions insertion and extraction. These may be explained by the facts that: (1) sub-micro $LiNi_xMn_{2-x}O_4$ (UACP) can provide better lithium ion diffusion pathways, that facilitate Li^+ intercalation kinetics, and in turn enhance cycle stability with less structural distortions at the surface; (2) smaller particles can provide more interfacial area for contact within the liquid electrolyte and hence can increase the opportunity for lithium ions to intercalate back into the host structure [30,31]; (3) the relatively porous powder morphology (see Fig. 4(b)) would help to release the stresses generated by the repetitive Li^+ intercalation. Therefore, we believe that ultrasonic-catalysis is an important factor to achieve higher capacity with good cycleability. The excellent recharge ability for the sub-micro spinels results from a homogeneous insertion/extraction reaction proceeding over the entire intercalation region. Moreover, an interesting thing is that the discharge capacity increases slightly in the initial stage and the electrode reaches a largest discharge capacity at *C*/3 discharge rate after several cycles as shown in Fig. 7(a) and (b), probably because the $LiNi_{0.5-x}Mn_{1.5+x}O_4$ electrode is not thoroughly wetted by the electrolyte. Once the intercalation and deintercalation process start, the volume of the electrode begins to expand and shrink, enabling the electrolyte to wet the $LiNi_{0.5-x}Mn_{1.5+x}O_4$ powders more thoroughly.

The cyclic voltammogram properties of $LiNi_{0.5-x}Mn_{1.5+x}O_4$ ($x<0.1$) spinel (UACP) at 1st, 15th and 30th cycles were tested. Cyclic voltammograms (sweep rate: 0.1 mV s^{-1}) in the potential region of 3.5–5.0 V are presented in Fig. 8.

The peaks in the CV curve from $LiNi_{0.5-x}Mn_{1.5+x}O_4$ correspond to the oxidation of Mn^{3+}, Ni^{2+}, and Ni^{3+}. However, the two cathodic peaks are overlapped to a broad peak because of very narrow potential gap between peaks and look like one broad peak [32]. The discharge capacity in each cycle can be estimated from the area of the reduction peaks. In the 15th and

Table 1
Cycle performance datum of the prepared powders at different discharge rates for the 1st cycle and the 100th cycle

Samples	Discharge rate	Initial discharge capacity (mAh g^{-1})	Discharge capacity after 100 cycles (mAh g^{-1})	Capacity retention ratio (%)[a]
$LiNi_{0.5-x}Mn_{1.5+x}O_4$ (UACP)	*C*/3	130.2	129.9	99.8
	1*C*	119.0	105.0	88.2
	2*C*	110.0	80.8	73.5
$LiNi_{0.5-x}Mn_{1.5+x}O_4$ (co-precipitation)	*C*/3	128.0	116.1	90.7
	1*C*	114.3	91.9	80.4
	2*C*	101.8	68.2	67.0

[a] The capacity retention ratio is according to the equation: $(C_{100}/C_1) \times 100\%$, where C_{100} is the discharge capacity after 100 cycles and C_1 is the initial discharge capacity.

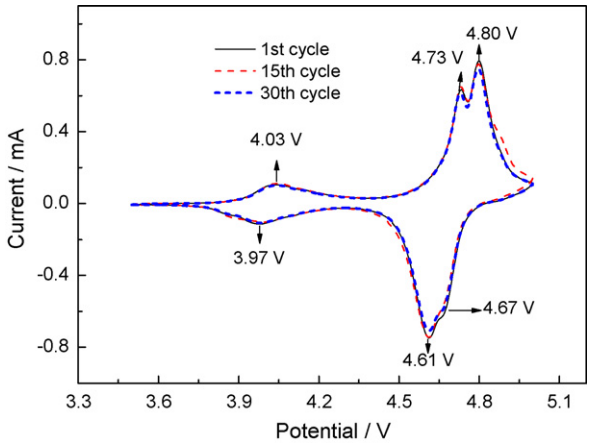

Fig. 8. Cyclic voltammograms of $LiNi_{0.5-x}Mn_{1.5+x}O_4$ ($x<0.1$) (UACP) cell at 1st, 15th and 30th cycles between 3.5 and 5 V with a scanning rate 0.1 mV s^{-1}.

30th cycle, the area is almost equal to that in the first cycle, indicating that the discharge capacity does not fade, which is in agreement with the result obtained from the charge and discharge test in Fig. 7(b) (*C*/3 discharge rate). CV curve implies that Ni-doped spinel synthesized by UACP method enhances both reversibility and cycle capability. Consequently, it is inferred that the $LiNi_{0.5-x}Mn_{1.5+x}O_4$ electrode synthesized by UACP method has high cycle performance because of the mechanism of ultrasonic-catalysis.

3.5. Mechanism of ultrasonic-catalysis

The mechanism of ultrasonic-catalysis is not related with the direct interaction between sound waves and molecules, but the liquid vacuum process. When air bubbles collapse, the local temperature will be above 5000 K and the local pressure will be up to 5×10^7 Pa. Meanwhile, the change rate of temperature is about 109 K s^{-1} and there are intense bow wave and 400 km h^{-1} current, which offers a very special physical condition [33]. The Kelvin formula is as follows:

$$\ln \frac{p_r}{p_0} = \frac{2\sigma M}{r\rho RT}, \qquad \ln \frac{x_r}{x_0} = \frac{2\sigma M}{r\rho RT}$$

where p_0 is the saturated vapor pressure of planar liquid level; p_r the saturated vapor pressure of curly liquid level; σ the surface tension of liquid; ρ the density of liquid; M the mole mass of liquid; r the radius of curvature of liquid; x_r and x_0 are the dissolvability of smaller crystalline grain and general crystalline grain, respectively.

According to the Kelvin formula, the dissolvability and saturated vapor pressure of small particles are very bigger than those of big particles. Consequently, under normal condition, the sediment of big particles is easy to form, and the small particles are difficult to form because of the big degree of supersaturation of the solution. However, the condition of high temperature and pressure formed by ultrasonic-catalysis can provide enough energy to form the sediment of small particles, and improve the formation rate of the sediments, which can also lead to the formation of the small particles. The condition of high temperature formed by ultrasonic-catalysis greatly reduces the specific surface free energy of the small particles, and restrains the growth of the crystal nucleus, so the intense bow wave formed by ultrasonic-catalysis makes the sediments exist as the small particles. The precursors of small particles reduce the activation energy formed $LiNi_{0.5-x}Mn_{1.5+x}O_4$ spinel during the calcinations, which increases reaction rate. Therefore, ultrasonic wave treating can significantly increase physicochemical properties, and this comment is well consistent with the experimental results mentioned above in this paper.

4. Conclusions

A good quality $LiNi_{0.5-x}Mn_{1.5+x}O_4$ ($x<0.1$) cathode material was successfully synthesized by ultrasonic-assisted co-precipitation method. The $I(3\,1\,1)/I(4\,0\,0)$ ratio, as well as the lattice parameter and the smaller size of the materials (UACP) are expected to show better electrochemical performance. Mn oxidation state in $LiNi_{0.5-x}Mn_{1.5+x}O_4$ ($x<0.1$) is between +3 and +4, and Ni oxidation state of $LiNi_{0.5-x}Mn_{1.5+x}O_4$ ($x<0.1$) is close to +2. $LiNi_{0.5-x}Mn_{1.5+x}O_4$ ($x<0.1$) obtained by UACP method has an octahedral morphology with well ordered direction, and consists of smaller particles, which is less than 200 nm. Compared with the $LiNi_xMn_{2-x}O_4$ synthesized by co-precipitation method, the Ni-doped spinel obtained from the simple UACP method has a larger initial discharge capacity and much higher capacity retention rate at different discharge rates after 100 cycles. $LiNi_{0.5-x}Mn_{1.5+x}O_4$ ($x<0.1$) obtained by UACP method at *C*/3 discharge rate exhibits superior capacity retention upon cycling, and it also shows well high current discharge performance. Ni-doped spinel synthesized by UACP method enhances both reversibility and cycle capability. The ultrasonic-assisted co-precipitation method is a better alternative than the traditional preparation method for synthesizing lithium-ion battery cathode materials.

Acknowledgements

The authors gratefully acknowledge financial support from Harbin Institute of Technology. The authors also thank Dr. Ying Wang of Institute of Chemistry Chinese Academy of Sciences for his helpful discussion on the experimental techniques.

References

[1] Y.P. Fu, Y.H. Su, C.H. Lin, S.H. Wu, J. Mater. Sci. 41 (2006) 1157.
[2] Y.C. Sun, Z.X. Wang, X.J. Huang, L.Q. Chen, J. Power Sources 132 (2004) 161.
[3] Y.-K. Sun, K.-J. Hong, J. Prakash, K. Amine, Electrochem. Commun. 4 (2002) 344.
[4] J. Molenda, J. Marzec, K. Świerczek, D. Pałubiak, W. Ojczyk, M. Ziemnicki, Solid State Ionics 175 (2004) 297.
[5] Y. Ein-Eli, J.T. Vaughey, M.M. Thackeray, S. Mukerjee, X.Q. Yang, J. McBreen, J. Electrochem. Soc. 146 (3) (1999) 908.
[6] H.S. Fang, Z.X. Wang, X.H. Li, H.J. Guo, W.J. Peng, J. Power Sources 153 (2006) 174.
[7] Q. Zhong, A. Bonakdarpour, M. Zhong, Y. Gao, J.R. Dahn, J. Electrochem. Soc. 144 (1997) 205.
[8] Y. Idemoto, H. Sekine, K. Ui, N. Koura, Solid State Ionics 176 (2005) 299.

[9] S.-T. Myung, S. Komaba, N. Kumagai, H. Yashiro, H.-T. Chung, T.-H. Cho, Electrochim. Acta 47 (2002) 2543.
[10] Y.S. Lee, Y.K. Sun, S. Ota, T. Miyashita, M. Yoshio, Electrochem. Commun. 4 (2002) 989.
[11] J.-H. Kim, S.-T. Myung, Y.-K. Sun, Electrochim. Acta 49 (2004) 219.
[12] S.H. Park, S.W. Oh, S.T. Myung, Y.K. Sun, Electrochem. Solid State Lett. 7 (2004) A451.
[13] P. Shen, Y. Huang, L. Liu, D. Jia, Z. Guo, J. Solid State Electrochem. 10 (2006) 929.
[14] T.F. Yi, X.G. Hu, K. Gao, J. Power Sources 162 (2006) 636.
[15] C.P. Vicente, J.M. Lloris, J.L. Tirado, Electrochim. Acta 49 (2004) 1963.
[16] Y.J. Wei, K.W. Nam, K.B. Kim, G. Chen, Solid State Ionics 177 (2006) 29.
[17] Y.S. Lee, N. Kumada, M. Yoshio, J. Power Sources 96 (2001) 376.
[18] Z. Li, C. Wang, X. Ma, L. Yuan, J. Sun, Mater. Chem. Phys. 91 (2005) 36.
[19] N. Treuil, C. Labrugere, M. Menetrier, J. Portier, G. Campet, A. Deshayes, J.-C. Frison, S.-J. Hwang, S.-W. Song, J.-H. Choy, J. Phys. Chem. B 103 (1999) 2100.
[20] M. Borges-Soares, F. Menes, R. Fontaine, R. Caillat, J. Microsc. Spectrosc. Electron. 8 (1983) 93.
[21] L. Hernan, J. Morales, L. Sanchez, J. Santos, E.R. Castellon, Solid State Ionics 133 (2000) 179.
[22] K.S. Kim, N. Winograd, Surf. Sci. 43 (1974) 625.
[23] K.M. Shaju, G.V. Subba Rao, B.R.V. Chowdari, Solid State Ionics 152/153 (2002) 69.
[24] T. Eriksson, T. Gustafsson, J.O. Thomas, Electrochem. Solid State Lett. 5 (2002) A35.
[25] A. Caballero, M. Cruz, L. Hernan, M. Melero, J. Morales, E.R. Castellon, J. Power Sources 150 (2005) 192.
[26] J.F. Moulder, W.F. Stickle, P.E. Sool, K.D. Bomber, Handbook of X-ray Photoelectron Spectroscopy, Perkin-Elmer, Eden Prairie, 1992.
[27] A.N. Mansour, Surf. Sci. Spectra 3 (1996) 279.
[28] A. Caballero, L. Hernan, M. Melero, J. Morales, M. Angulo, J. Electrochem. Soc. 152 (2005) A6.
[29] Y. Gao, K. Myrtle, M. Zhang, J.N. Reimers, J.R. Dahn, Phys. Rev. B 54 (1996) 16679.
[30] C.Z. Lu, G. Ting-Kuo Fey, J. Phys. Chem. Solids 67 (2006) 756.
[31] T.F. Yi, D.L. Wang, K. Gao, X.G. Hu, J. Rare Earths 23 (Suppl.) (2005) 209.
[32] K. Takahashi, M. Saitoh, M. Sano, M. Fujita, K. Kifune, J. Electrochem. Soc. 151 (2004) A173.
[33] E.B. Flint, K.S. Suslick, Science 253 (1991) 1397.